

Article

Coupled Chiral Optical Tamm States in Cholesteric Liquid Crystals

Maxim V. Pyatnov ^{1,*}, Ivan V. Timofeev ^{1,2}, Stepan Ya. Vetrov ^{1,2} and Natalya V. Rudakova ¹

¹ Siberian Federal University, Institute of Engineering Physics and Radio Electronics, 660041 Krasnoyarsk, Russia;

² Kirensky Institute of Physics, Federal Research Center "Krasnoyarsk Scientific Center, Russian Academy of Sciences, Siberian Branch", 660036 Krasnoyarsk, Russia;

* Correspondence: MaksPyatnov@yandex.ru;

Academic Editor: name

Version August 29, 2018 submitted to Journal Not Specified

Abstract: The modes formed by two coupled chiral optical Tamm states localized at the interfaces between a photonic cholesteric liquid crystal conjugated with polarization-preserving anisotropic mirrors have been analytically and numerically investigated. These modes are only excited at the diffracting polarization of incident light. As the cholesteric layer thickness decreases, the spectral splitting of the localized state frequency is observed. The splitting value depends on the crystal layer thickness. At the nondiffracting circular polarization, the localized modes are not excited and the system becomes similar to the Fabry–Pérot cavity containing an anisotropic helical structure.

Keywords: cholesteric liquid crystal; optical Tamm states; localization; transmission spectrum; optical devices

1. Introduction

The optical Tamm state (OTS) attracts particular attention of researches among various surface localized optical states. This is a mode localized at the interface between two highly reflecting media, which exponentially decays to both of them [1,2]. If one of the media is a metal, the OTS is called a Tamm plasmon [3]. Such a localized mode at the interface between two materials can be excited by both TE and TM linear polarizations at any light incidence angles. The OTS manifests itself in experiments as a narrow resonance in the transmittance or reflectance spectrum of the sample. The interest in the OTSs and Tamm plasmons is due to their possible applications in lasers and emitters [4–7], sensors [8,9], photovoltaic devices [10], etc. Lately, Cheng et. al. demonstrated a liquid crystal-tuned Tamm-plasmon resonance device [11].

The OTSs can be strongly coupled with each other or with the resonances of different nature, including cavity modes, exciton polaritons, and surface plasmons [12–16]. Such hybrid modes are characterized by anticrossing of the resonances upon tuning a position of one of them.

It seems promising to use a soft matter as a photonic material. Cholesteric liquid crystals (CLCs) are the well-proven elements of optical systems. These are birefringent materials with the chirality property. The alignment of extended CLC molecules is characterized by a continuously rotating director. Similar to one-dimensional photonic crystals, cholesterics have a photonic band gap [17]. However, the position and width of their band gap can be easily changed using external factors. In contrast to scalar photonic-crystal materials or distributed Bragg reflectors, CLCs have the only band gap at the normal incidence of light. This band gap only exists for the light with the diffracting circular polarization coinciding with the twisting of a cholesteric helix. The circularly polarized radiation of the opposite direction (nondiffracting polarization) is not reflected from such a structure.

32 In contrast to the case of metals or conventional dielectrics, the circularly polarized radiation
 33 reflected from the CLC preserves the sign of its polarization handedness. Therefore, obtaining a Tamm
 34 plasmon localized between the CLC and metallic layer or the OTS localized between the CLC and
 35 distributed Bragg reflector is a challenging problem. It can be solved in two ways. The first way is to
 36 use an additional anisotropic layer, e.g., a quarter-wave phase plate [18,19], an oppositely twisted CLC
 37 [20], or a planar anisotropic defect in the CLC [21]. In this case, however, the observed localized states
 38 are not called Tamm states. The other way is to use a polarization-preserving (handedness-preserving
 39 or chiral) mirror instead of a conventional one. These mirrors retain not only the handedness, but also
 40 the ellipticity magnitude upon reflection. The state at the polarization-preserving mirror–CLC interface
 41 was described in the low [22] and finite [23] anisotropy approximations of a cholesteric crystal and
 42 named a chiral OTS. The metasurfaces can have the properties of handedness-preserving mirrors [24].

43 In this work, we examine the coupling between two chiral OTSs localized at both CLC boundaries.

44 2. Model Description

45 The system under study is presented in Figure 1. The right-handed CLC is sandwiched between
 46 two identical polarization-preserving anisotropic mirrors (PPAMs). The CLC parameters used in the
 47 simulation were ordinary and extraordinary refractive indices of $n_o = 1.54$ and $n_e = 1.71$ and a helix
 48 pitch of $p = 0.4 \mu\text{m}$. These parameters are typical of the mixture of a Merck S-811 chiral additive
 49 and a nematic liquid crystal [25]. The CLC layer thickness is specified by parameter d . To meet the
 50 boundary conditions, we hereinafter assume the CLC to have an integer number of periods (the period
 51 is a distance of the director rotation by angle π). The PPAMs consist of alternating uniaxial dielectric
 52 layers with refractive indices n_e^m and n_o^m . Each layer is rotated relative to the previous one by 90° .
 53 The mirrors contain $N = 10$ periods. The PPAM period thickness is $2a = 0.2 \mu\text{m}$. As was shown previously,
 54 such anisotropic mirrors can preserve the polarization of the radiation falling onto them [26]. This
 55 is a necessary condition for forming the OTS at the CLC boundary. In Reference [27], a chiral OTS
 56 is described at the CLC and PPAM interface. The angles between the CLC optical axes and adjacent
 57 mirror layers are hereinafter referred to as ψ and φ , respectively. Below, we assume $\psi = \pi/4$. The
 58 structure is surrounded by a medium with the refractive index equal to the averaged CLC refractive
 59 index next equal $n = (n_e + n_o)/2$.

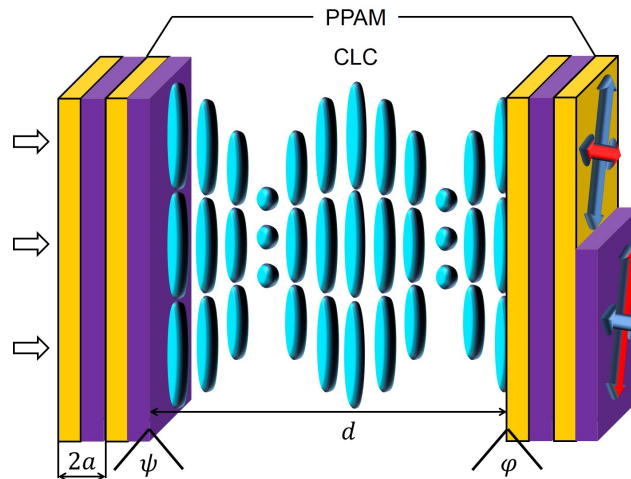


Figure 1. Schematic of the structure. Color arrows show the direction of optical axes of the PPAM layers. Each PPAM consists of 10 periods.

60 We assumed the refractive indices to be $n_e = n_e^m$ and $n_o = n_o^m$; i. e., the CLC refractive indices
 61 are equal to the corresponding refractive indices of the PPAM layers. At these parameters, the centers
 62 of the CLC and PPAM band gaps coincide. As was demonstrated in [22,23], under this condition at

63 $\psi = \pi/4$, the OTS manifests itself in the spectrum exactly at the band gap center. At $\varphi = \psi = \pi/4$,
 64 the boundary conditions are satisfied, which leads to the possibility of exciting two OTSs localized
 65 at both boundaries of a confined CLC. Both OTSs are symmetric and therefore should appear in the
 66 spectrum at the same frequency; however, since these states are coupled through a finite CLC layer,
 67 the frequency degeneracy is eliminated and two peaks arise in the spectrum at similar frequencies. At
 68 the integer number of CLC periods, the angle between the optical axes of the PPAM layers adjacent to
 69 the CLC from the left and right is $\varphi + \psi = \pi/2$. These layers are shown by different colors in Figure 1.

70 3. Results and Discussion

71 Figure 2 shows the transmittance spectra for the circular polarizations of incidence light as a
 72 function of the CLC width, which were simulated using the 4×4 Berreman matrix [28]. One can see
 73 the behavior of the spectrum at the right-handed circular polarization of the incident light. At the large
 74 CLC thicknesses, the transmittance peak corresponding to the OTS is observed for this polarization.
 75 This fact is confirmed by the spatial distribution of the squared absolute value of electric field $|E|^2(z)$ at
 76 a wavelength of 650 nm (the blue line in Figure 3a). The field is localized with the maxima at the CLC
 77 boundary. Since the light falls from the left and the CLC has a high reflectivity, the field is localized
 78 stronger on the left CLC boundary. As the distance to the boundary increases, the fields exponentially
 79 decay.

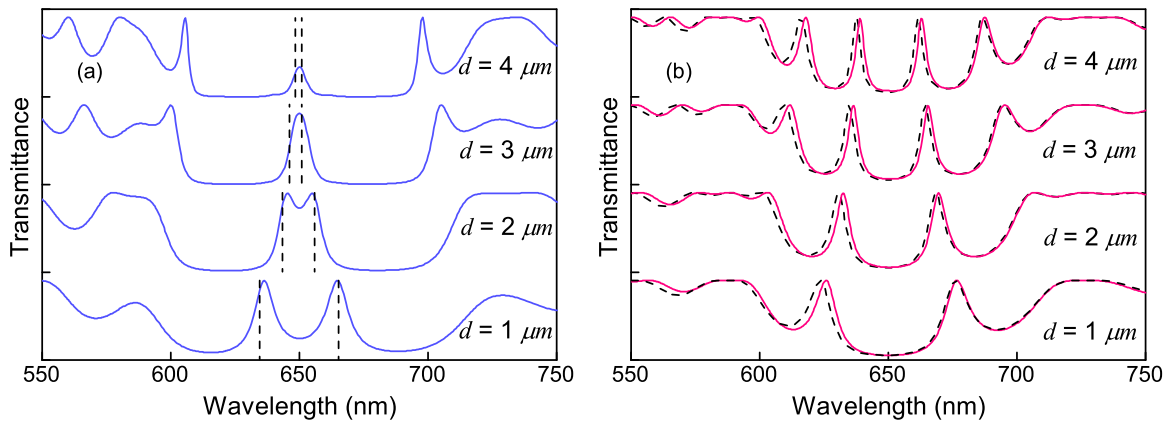


Figure 2. Dependence of the transmittance spectrum for (a) the right- and (b) left-handed circular polarizations of the incident light on CLC layer thickness d . Dashed lines in Figure 2a show the OTS spectral positions calculated using formula (9) and dashed lines in Figure 2b, transmittance spectra for the nondiffracting polarization analytically calculated using formula (11); $\varphi = \pi/4$.

80 A decrease in the CLC layer thickness leads to the overlap of the OTS electromagnetic fields
 81 (Figure 3b), which eliminates the degeneracy. The frequency splits and two transmittance peaks arise
 82 in the spectrum.

83 The specific feature of the CLC is the dependence of the spectrum on the polarization of the
 84 incident light. The nondiffracting polarization opposite to the CLC twisting direction is not reflected
 85 from the cholesteric. Since the investigated system contains a right-handed CLC, the OTS does not
 86 occur for the left-handed circular polarization. At this polarization, the structure under study becomes
 87 similar to the Fabry–Pérot cavity and resonances arise in its transmittance spectrum. The number of
 88 these resonances depends on the distance between the mirrors (Figure 2b). The $|E|^2(z)$ dependence for
 89 such a circular polarization of the incident light (the red line in Figure 3) confirms that the peaks for
 90 the left-handed circular polarization correspond to the cavity modes. Thus, the transmittance spectra
 91 for the circular polarizations of the incident light are different. At the non-circular polarizations of the
 92 incident light, the peaks arise at all frequencies.

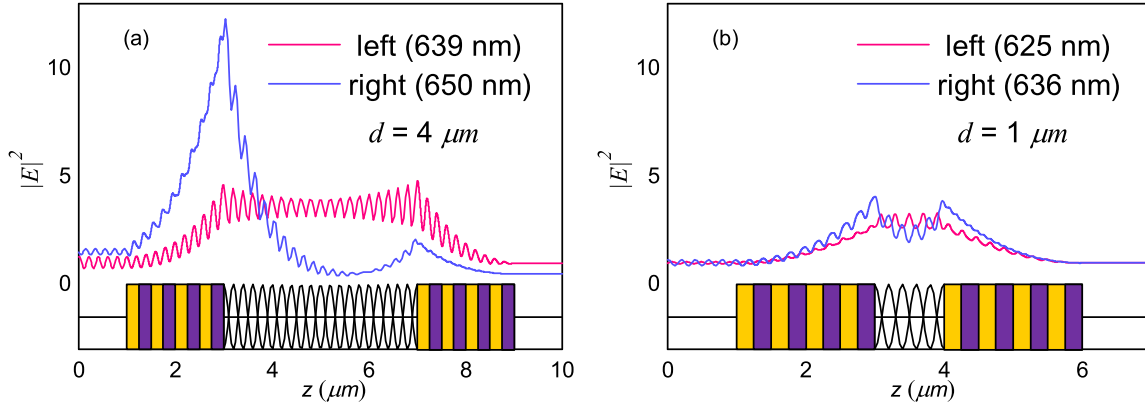


Figure 3. Spatial distribution of the local electric field intensity in the structure for the circular polarizations of incidence light. (a) $d = 4 \mu\text{m}$ and (b) $d = 1 \mu\text{m}$. Each PPAM consists of 10 periods; $\varphi = \pi/4$.

93 In addition to the numerical simulation, we developed the analytical description of the system.
 94 For the scalar systems, the equation for a single OTS localized at the interface between two media has
 95 the following form for the arbitrary wave polarization [3]:

$$r_L r_R e^{2i\Phi} = 1. \quad (1)$$

96 Here, r_L and r_R are the amplitude reflectances of the left and right mirrors, respectively, and Φ is the
 97 phase variation for the wave transmitted through the layer separating the mirrors. Let us consider the
 98 occurrence of a single chiral OTS at the CLC/PPAM interface. We assumed Equation (1) to be valid
 99 at the normal incidence for the diffracting circular polarization, if the relation to the nondiffracting
 100 polarization is ignored. Therefore, for the chiral OTS, Φ should be replaced by φ .

101 The amplitude reflectance of the left mirror, which is a CLC, is [30]:

$$r_L = r_{CLC} = \frac{i\delta \sin qd}{((q\tau/\kappa^2) \cos qd + i((\tau/2\kappa)^2 + (q/\kappa)^2 - 1) \sin qd)}. \quad (2)$$

102 Here, $\delta = \frac{(n_e^2 - n_0^2)}{(n_e^2 + n_0^2)}$, $\kappa = \frac{\omega \sqrt{(n_e^2 + n_0^2)/2}}{c}$, and $\tau = \frac{4\pi}{p}$ is the CLC reciprocal lattice vector. The vector of
 103 the wave diffracting in the CLC is

$$q = \kappa \sqrt{1 + (\tau/2\kappa)^2 - \sqrt{(\tau/\kappa)^2 + \delta^2}}. \quad (3)$$

104 For the right mirror, the reflectance of the layered structure with N periods is determined as [31]

$$r_R = r_{PPAM} = \frac{CU_{N-1}}{AU_{N-1} - U_{N-2}}, \quad (4)$$

105 where $U_N = \frac{\sin 2a(N-1)K}{\sin 2aK}$, $K = \frac{1}{2a} \arccos(\frac{A+D}{2})$ is the Bloch wavenumber.

106 Since we only investigate the case of the normal incidence, elements A , B , C , and D of the transfer
 107 matrix for one cell, which relate the plane wave amplitudes in the first unit-cell layer to the amplitudes
 108 in the neighboring unit cell, can be written in the form

$$A = e^{ik_{1z}a} \left[\cos k_{2z}a + \frac{1}{2}i \left(\frac{k_{2z}}{k_{1z}} + \frac{k_{1z}}{k_{2z}} \right) \sin k_{2z}a \right]; \quad (5)$$

$$B = e^{-ik_{1z}a} \left[\frac{1}{2}i \left(\frac{k_{2z}}{k_{1z}} - \frac{k_{1z}}{k_{2z}} \right) \sin k_{2z}a \right];$$

$$C = e^{ik_{1z}a} \left[-\frac{1}{2}i \left(\frac{k_{2z}}{k_{1z}} - \frac{k_{1z}}{k_{2z}} \right) \sin k_{2z}a \right];$$

$$D = e^{-ik_{1z}a} \left[\cos k_{2z}a - \frac{1}{2}i \left(\frac{k_{2z}}{k_{1z}} + \frac{k_{1z}}{k_{2z}} \right) \sin k_{2z}a \right],$$

109 where $k_{1z} = (\omega/c)n_e^2$, $k_{2z} = (\omega/c)n_o^2$ are the wave vectors for the first and second media, respectively,
 110 and $2a$ is the PPAM period. The resulting equation for the chiral OTS localized at the interface between
 111 two media with reflectances r_{PPAM} and r_{CLC} and the angle φ between the optical axes is

$$r_{PPAM}r_{CLC}e^{2i\varphi} = 1. \quad (6)$$

112 The solution of this equation at the center of the Bragg reflection of the mirrors leads to the result,
 113 in which at the angle $\varphi = \pi/4$, the single chiral OTS is excited exactly at the CLC band gap center,
 114 which is consistent with the predictions from [22,23]. The equation for the coupled chiral OTSs should
 115 contain a term responsible for the coupling value. Obviously, it should be proportional to the CLC
 116 thickness and reflectance. We suggested that it can be written in the form $\pm \frac{t_{CLC}}{r_{CLC}}$, as was made for
 117 scalar structures in [12,29]. The amplitude transmittance of the CLC is determined as [30]

$$t_{CLC} = \frac{e^{i\tau d/2}((q\tau/\kappa^2))}{((q\tau/\kappa^2) \cos qd + i((\tau/2\kappa)^2 + (q/\kappa)^2 - 1) \sin qd)}. \quad (7)$$

118 Thus, for the coupled chiral OTSs, we have

$$1 \pm \frac{t_{CLC}}{r_{CLC}} = r_{PPAM}r_{CLC}e^{2i\varphi}. \quad (8)$$

119 Near the Bragg frequency, the amplitudes r_{PPAM} and r_{CLC} are almost unity. We denote the phase
 120 of expression $\pm \frac{t_{CLC}}{r_{CLC}}$ by θ_{\pm} and the phases of the waves reflected from the PPAM and CLC by φ_{PPAM}
 121 and φ_{CLC} and write Equation (8) in the form

$$\theta_{\pm} = \varphi_{PPAM} + \varphi_{CLC} + 2\varphi. \quad (9)$$

122 This equation allows us to determine the eigenfrequencies of the coupled chiral OTSs. The
 123 frequencies calculated in this manner at different CLC thicknesses d (dashed lines in Figure 2a) are
 124 consistent with the simulation data the solid line in Figure 2a).

125 If the CLC layer is thick and the angles ψ and φ are equal to $\pi/4$, two OTSs are excited in the
 126 system, which occur in the spectrum at the same frequency. Varying one of the angles, one can tune a
 127 spectral position of one of the OTSs. We numerically investigated the interaction between the OTSs
 128 localized at the both CLC boundaries as a function of the angle φ (Figure 4). The peak corresponding
 129 to the OTS localized at the left CLC boundary did not change its wavelength. At $\varphi = \pi/4$, the
 130 two frequencies coincide and the splitting occurs. Upon variation in φ , the spectrum demonstrates
 131 anticrossing typical of the bound states. White lines in the figures show the solution of Equation (6) for
 132 single OTSs.

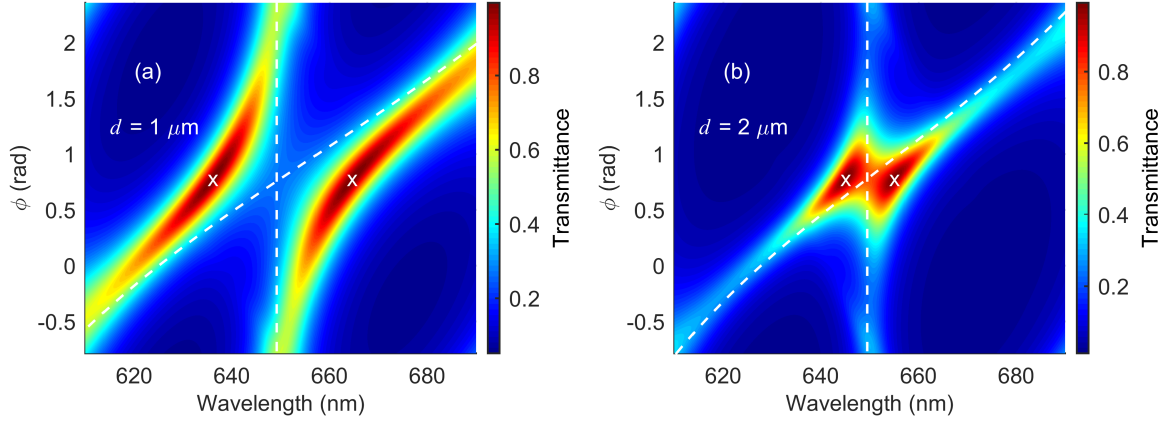


Figure 4. Transmittance of the structure from Figure 1 as a function of angle ϕ at different CLC widths d . (a) $d = 1 \mu\text{m}$ and (b) $d = 2 \mu\text{m}$. White lines show positions of single OTSs calculated using Equation (6). The crosses correspond to OTS wavelengths for $\phi = \pi/4$.

133 The transmittance spectrum at the normal incidence of the left-handed nondiffracting polarization,
 134 at which the OTSs are not excited (Figure 2b), can be found using the well-known expression for the
 135 transmittance of the Fabry–Pérot cavity [32]

$$T_{FP} = \frac{(1 - |r_{PPAM}|^2)^2}{(1 - |r_{PPAM}|^2)^2 + 4|r_{PPAM}|^2 \sin^2(\delta/2)} \quad (10)$$

136 In the investigated model, $\delta/2$ should be written in the form

$$\delta/2 = \varphi_{PPAM} - \pi/2 - \omega nd/c \quad (11)$$

137 where n is the average refractive index of the CLC. The transmittance spectra for the structure with the
 138 left-handed nondiffracting polarization calculated using Equation (10) are shown by dashed lines in
 139 Figure 2b.

140 An important advantage of the CLC as a photonic material is its high sensitivity to external fields.
 141 The electromagnetic field and temperature [33] can change the CLC helix pitch or even transform it
 142 to another aggregate state. As the helix pitch changes, the peaks shift and the CLC and PPAM band
 143 gaps no longer overlap. Thus, the OTSs will not be excited for the diffracting polarization and the
 144 system will turn to the Fabry–Pérot cavity filled with anisotropic helical structures [34,35]. The spectra
 145 for both circular polarizations will become identical and doublets will arise in them. After the phase
 146 transition of the CLC to the isotropic state, the system transforms to a conventional Fabry–Pérot cavity.

147 4. Conclusions

148 We demonstrated the existence of the modes caused by coupling of two chiral optical Tamm states
 149 localized at the interface between the CLC and anisotropic mirrors. The mirrors represent uniaxial
 150 layered structures, in which each layer is rotated by 90° relative to the previous one. Such a structure is
 151 polarization-preserving. The need for these mirrors is caused by the polarization properties of the CLC.
 152 The investigated modes are only excited at the diffracting polarization of the incident light. As the CLC
 153 layer thickness decreases, the OTS frequency spectral split is observed. The split value depends on the
 154 layer thickness. We found analytically and numerically the frequencies of the spectral manifestation of
 155 the chiral OTSs. Varying the angle between the CLC and PPAM optical axes, one can control the OTS
 156 coupling value, thereby tuning the transmittance spectrum of the structure. At the opposite circular
 157 polarization, which does not reflect from the CLC, the OTSs are not excited and the system becomes
 158 analogous to a Fabry–Pérot cavity filled with an anisotropic helical structure. The possible tuning of
 159 the spectra by external factors was discussed.

160 **Author Contributions:** M.V.P. performed the calculations, visualized the results and drafted the manuscript. I.V.T.
161 and N.V.R. helped with software, methods and checked analytical expressions, S.Ya.V. supervised the whole study
162 and finalized the manuscript

163 **Funding:** This research was funded by Russian Foundation for Basic Research, Government of Krasnoyarsk
164 Territory, Krasnoyarsk Region Science and Technology Support Fund to the research projects No. 17-42-240464,
165 18-42-243025.

166 **Conflicts of Interest:** The authors declare no conflict of interest.

167 References

- 168 1. Goto, T.; Dorofeenko, A.V.; Merzlikin, A.M.; Baryshev, A.V.; Vinogradov, A.P.; Inoue, M.; Lisyansky, A.A.;
169 Granovsky, A.B. Optical Tamm states in one-dimensional magnetophotonic structures. *Phys. Rev. Lett.* **2008**,
170 *101*, 113902, DOI:10.1103/PhysRevLett.101.113902
- 171 2. Kavokin, A.V.; Shelykh I.A.; Malpuech, G. Lossless interface modes at the boundary between two periodic
172 dielectric structures. *Phys. Rev. B* **2005**, *72*, 233102, DOI:10.1103/PhysRevB.72.233102
- 173 3. Kaliteevski, M.A.; Iorsh, I.; Brand, S.; Abram, R.A.; Chamberlain, J.M.; Kavokin, A.V.; Shelykh, I.A. Tamm
174 plasmon-polaritons: Possible electromagnetic states at the interface of a metal and a dielectric Bragg mirror.
175 *Phys. Rev. B* **2007**, *76*, 165415, DOI:10.1103/PhysRevB.76.165415
- 176 4. Symonds, C.; Lheureux, G.; Hugonin, J.-P.; Greffet, J.-J.; Laverdant, J.; Brucoli, G.; Lemaitre, A.; Senellart, P.;
177 Bellessa, J. Confined Tamm plasmon lasers. *Nano Lett.* **2013**, *13*, 3179-3184, DOI:10.1021/nl401210b
- 178 5. Jiménez-Solano, A.; Galisteo-López, J.F.; Míguez, H. Flexible and Adaptable Light-Emitting Coatings for
179 Arbitrary Metal Surfaces based on Optical Tamm Mode Coupling. *Adv. Opt. Mat.* **2017**, *6*, 1700560,
180 DOI:10.1002/adom.201700560
- 181 6. Yang, Z.-Y.; Ishii, S.; Yokoyama, T.; Dao, T.D.; Sun, M.-G.; Pankin, P.S.; Timofeev, I.V.; Nagao, T.; Chen, K.-P.
182 Narrowband wavelength selective thermal emitters by confined tamm plasmon polaritons. *ACS Phot.* **2017**,
183 *4*, 2212-2219, DOI:10.1021/acsphotonics.7b00408
- 184 7. Zhang, X.-L.; Feng, J.; Han, X.-C.; Liu, Y.-F.; Chen, Q.-D.; Song, J.-F.; Sun, H.-B. Hybrid Tamm
185 plasmon-polariton/microcavity modes for white top-emitting organic light-emitting devices. *Optica* **2015**, *2*,
186 579-584, DOI:10.1364/OPTICA.2.000579
- 187 8. Huang, S.-G.; Chen, K.-P.; Jeng, S.-C. Phase sensitive sensor on Tamm plasmon devices. *Opt. Mat. Exp.* **2017**,
188 *72*, 1267-1273, DOI:10.1364/OME.7.001267
- 189 9. Kumar, S.; Maji, P.S.; Das, R. Tamm-plasmon resonance based temperature sensor in a Ta2O5/SiO2 based
190 distributed Bragg reflector. *Sens. Act. A: Phys.* **2017**, *260*, 10-15, DOI:10.1016/j.sna.2017.03.038
- 191 10. Zhang, X.-L.; Song, J.-F.; Li, X.-B.; Feng, J.; Sun, H.-B. Optical Tamm states enhanced broad-band absorption
192 of organic solar cells. *Appl. Phys. Lett.* **2012**, *101*, 243901, DOI:10.1063/1.4770316
- 193 11. Cheng, H.-C.; Kuo, C.-Y.; Hung, Y.-J.; Chen, K.-P.; Jeng, S.-C. Liquid-Crystal Active Tamm-Plasmon Devices.
194 *Phys. Rev. Appl.* **2018**, *9*, 064034, DOI:10.1103/PhysRevApplied.9.064034
- 195 12. Kaliteevski, M. Brand, S.; Abram, R.A.; Iorsh, I. Kavokin, A.V. Shelykh, I.A. Hybrid states of Tamm plasmons
196 and exciton polaritons. *Appl. Phys. Lett.* **2009**, *95*, 251108, DOI:10.1063/1.3266841
- 197 13. Rahman, S.K.S.-U.; Klein, T.; Klemmt, S.; Gutowski, J.; Hommel, D.; Sebald, K. Observation of a hybrid state
198 of Tamm plasmons and microcavity exciton polaritons. *Sci. Rep.* **2016**, *6*, 34392, DOI:10.1038/srep34392
- 199 14. Afinogenov, B.I.; Bessonov, V.O.; Nikulin, A.A.; Fedyanin, A.A. Observation of hybrid state of Tamm and
200 surface plasmon-polaritons in one-dimensional photonic crystals. *Appl. Phys. Lett.* **2013**, *103*, 061112,
201 DOI:10.1063/1.4817999
- 202 15. Vetrov, S.Ya.; Bikbaev, R.G.; Timofeev, I.V. Optical Tamm states at the interface between a photonic crystal
203 and a nanocomposite with resonance dispersion. *JETP* **2013**, *117*, 988-998, 10.1134/S1063776113140185
- 204 16. Pankin, P.S.; Vetrov, S.Ya.; Timofeev, I.V. Tunable hybrid Tamm-microcavity states. *JOSA B* **2017**, *34*, 2633-2639,
205 DOI:10.1364/JOSAB.34.002633
- 206 17. Blinov, L.M. *Structure and Properties of Liquid Crystals*. Springer, 2011; ISBN. 978-90-481-8829-1
- 207 18. Vetrov, S.Ya.; Pyatnov, M.V.; Timofeev, I.V. Surface modes in "photonic cholesteric liquid crystal-phase
208 plate-metal" structure. *Opt. Lett.* **2014**, *39*, 2743-2746, DOI:10.1364/OL.39.002743

- 209 19. Vetrov, S.Ya.; Pyatnov, M.V.; Timofeev, I.V. Spectral and polarization properties of a 'cholesteric liquid
210 crystal—phase plate—metal' structure. *J. Opt.* **2015**, *18*, 015103, DOI:10.1088/2040-8978/18/1/015103
- 211 20. Pyatnov, M.V.; Vetrov, S.Ya.; Timofeev, I.V. Localised optical states in a structure formed by two
212 oppositely handed cholesteric liquid crystal layers and a metal. *Liq. Cryst.* **2017**, *44*, 674-678,
213 DOI:10.1080/02678292.2016.1229055
- 214 21. Pyatnov, M.V.; Vetrov, S.Ya.; Timofeev, I.V. Localized optical modes in a defect-containing liquid-crystal
215 structure adjacent to the metal. *JOSA B* **2017**, *34*, 2011-2017, DOI:10.1364/JOSAB.34.002011
- 216 22. Timofeev, I.V.; Pankin, P.S.; Vetrov, S.Ya.; Arkhipkin, V.G.; Lee, W.; Zyryanov, V.Ya. Chiral optical Tamm
217 states: temporal coupled-mode theory. *Crystals* **2017**, *7*, 113, DOI:10.3390/cryst7040113
- 218 23. Timofeev, I.V.; Vetrov, S.Ya. Chiral optical Tamm states at the boundary of the medium with helical symmetry
219 of the dielectric tensor. *JETP Lett.* **2016**, *104*, 380-383, DOI:10.1134/S0021364016180119
- 220 24. Ding, F.; Wang, Z.; He, S.; Shalaev, V.M.; Kildishev, A.V. Broadband high-efficiency half-wave
221 plate: a supercell-based plasmonic metasurface approach. *ACS Nano* **2015**, *9*, 4111-4119,
222 DOI:10.1021/acs.nano.5b00218
- 223 25. Matsuhisa, Y.; Ozaki, R.; Yoshino, K.; Ozaki, M. High Q defect mode and laser action in one-dimensional
224 hybrid photonic crystal containing cholesteric liquid crystal. *Appl. Phys. Lett.* **2006**, *89*, 101109,
225 DOI:10.1063/1.2347114
- 226 26. Rudakova, N.V.; Timofeev, I.V.; Pankin, P.S.; Vetrov, S.Ya. Polarization-preserving anisotropic mirror on
227 the basis of metal–dielectric nanocomposite. *Bul. Rus. Ac. Sc.: Phys.* **2017**, *81*, 5-9, DOI:10.3103/S10
228 62873817010257
- 229 27. Rudakova, N.V.; Timofeev, I.V.; Bikbaev, R.G.; Pyatnov, M.V.; Vetrov, S.Ya.; Lee, W. Chiral Optical Tamm
230 states at the interface between a cholesteric and an all-dielectric polarization-preserving anisotropic mirror.
231 <https://arxiv.org/abs/1808.06243>
- 232 28. Berreman, D.W. Optics in stratified and anisotropic media: 4×4 -matrix formulation. *J. Opt. Soc. Am.* **1972**,
233 *62*, 502-510, DOI:10.1364/JOSA.62.000502
- 234 29. Iorsh, I.; Panicheva, P.V.; Slovinskii, I.A.; Kaliteevski, M.A. Coupled Tamm plasmons. *Tech. Phys. Lett.* **2012**,
235 *38*, 351-353, DOI:10.1134/S1063785012040074
- 236 30. Belyakov, V.A. *Diffraction optics of complex-structured periodic media*. Springer-Verlag, 1992; ISBN:
237 978-1-4612-4396-0
- 238 31. Yariv, A.; Yeh, P. *Optical waves in crystals*. Wiley New York, 1984; ISBN-13: 978-0471430810, ISBN-10:
239 0471430811
- 240 32. Haus, H.A. *Waves and fields in optoelectronics*. Prentice-Hall, 1984; ISBN-13: 9780139460531, ISBN-10:
241 0139460535
- 242 33. Dolganov P.V.; Gordeev S.O.; Dolganov V.K.; Bobrovsky A.Yu. Photo- and thermo-induced variation of
243 photonic properties of cholesteric liquid crystal containing azobenzene-based chiral dopant. *Mol. Cryst. Liq.*
244 *Cryst.* **2016**, *633*, 14-22, DOI:10.1080/15421406.2016.1177874
- 245 34. Zhuang, Z.; Patel, J.S. Behavior of cholesteric liquid crystals in a Fabry-Perot cavity. *Opt. Lett.* **1999**, *24*,
246 1759-1761, DOI:10.1364/OL.24.001759
- 247 35. Abdulhalim, I. Unique optical properties of anisotropic helical structures in a Fabry-Perot cavity. *Opt. Lett.*
248 **1999**, *31*, 3019-3021, DOI:10.1364/OL.31.003019